Characterization of Recent GPS Satellite Clock Jumps

Rebecca Wang*, Yu-Fang Lai*, Juan Blanch*, Dennis Akos**, Eric Phelts*, and Todd Walter*

*Stanford University
**University of Colorado Boulder

BIOGRAPHY

Rebecca Wang is a Ph.D. candidate at the Stanford GPS Lab. She received a B.S. in aerospace engineering from the University of Texas at Austin in 2020 and an M.S. in aeronautics and astronautics from Stanford University in 2022.

Frank Lai is a Ph.D. candidate at the Stanford GPS Lab. He received his B.S. in aeronautics and astronautics from National Cheng-Kung University in 2020 and his M.S. in aeronautics and astronautics from Stanford University in 2022.

Juan Blanch is a senior research engineer at Stanford University. He holds an M.S. in electrical engineering from Ecole Polytechnique in France and a Ph.D. in aeronautics and astronautics from Stanford University.

Dennis Akos is a Professor at the University of Colorado Boulder and director of the Radio Frequency and Satellite Navigation Laboratory. He received his Ph.D. in electrical and computer engineering from Ohio University.

Eric Phelts is a research engineer at Stanford University. He holds an M.S. and Ph.D. in mechanical engineering from Stanford University.

Todd Walter is a Professor at Stanford University and director of the Stanford GPS Lab. He received his B.S. in physics from Rensselaer Polytechnic Institute and his Ph.D. in applied physics from Stanford University.

ABSTRACT

This year, a new fault case presented in the January 25, January 28, and July 10, 2023 clock jumps in the GPS constellation. Fault events in the global navigation satellite system (GNSS) affect the accuracy of positioning solutions, but are accounted for through standardized specifications such as those provided in the GPS Standard Positioning Service Performance Standard (GPS SPS PS). However, performance characterization of new and existing satellites in the navigation constellation is necessary to both validate these specifications and inform future design improvements. The Wide Area Augmentation System (WAAS) observed the January 25 and July 10, 2023 faults exhibiting unexpected instantaneous jumps in its clock measurement at a one second sampling frequency affecting only the code phase component. However, the carrier phase component did not demonstrate the same jump. Through comparison of positioning solutions from several different receiver makes, it appeared that the carrier phase component was also affected by these jumps, but were not detected as expected by the carrier tracking loop in the WAAS receiver. Consequently, differences in signal tracking and logic between different receivers become apparent in light of this new anomalous event. This paper examines this fault in greater detail and reports insights into the reaction by receivers to the event which will also inform next-generation receiver signal tracking designs.

I. INTRODUCTION

Performance of the global navigation satellite system (GNSS) is characterized for the purpose of supporting high integrity navigation augmentation systems and algorithms. Errors in the positioning solutions provided from GNSS signals can come from a variety of sources, with two main sources being satellite ephemeris and clock errors. As the continuity, availability, and coverage of GNSS changes over time, characterizing the probability of fault occurrences must be continuously performed. In particular, the development of Advanced Receiver Autonomous Integrity Monitoring (ARAIM) requires stricter validation than its predecessor, RAIM, which provides only lateral, and not vertical, autonomous integrity monitoring (Walter and Blanch, 2015). Fault analyses of the navigation constellation is increasingly important.

On July 10, 2023, space vehicle number (SVN) 63 in the GPS constellation went into a faulted state. Within the typical GPS fault causes of ephemeris errors and clock errors, clock faults have usually been characterized by a ramp, or a slowly increasing error, until the fault definition is violated. The fault definition is the error magnitude that the satellite is allowed to have before violating the threshold set by the GPS Standard Positioning Service Performance Standard (GPS SPS PS) (Department of Defense, 2020). For the GPS constellation, the fault threshold is defined as the product of 4.42 and the user range accuracy (URA) value, which

is broadcast from the navigation message and most commonly takes on the value of 2.4 m. The GPS SPS PS also states that the probability of a satellite transitioning into an integrity-faulted state should not surpass 10^{-5} per hour. In this event, the error which exceeded the fault definition shows up in our analysis at first glance as a clock error. The clock error reaches -40 m and remains at this error value until correction; however, the signal first became untrackable before being set unhealthy. This same satellite also had a recent fault on January 25, 2023 and fault-like behavior shortly after on January 28, 2023. Given the performance history of the GPS constellation and the near 10-year fault-free time frame achieved between 2012-2022, two faults occurring within a six-month span on the same satellite is atypical (Wang and Walter, 2023). Furthermore, instantaneous clock jumps have not been observed on GPS since at least June 26, 2009; typically, clock errors are characterized by a gradual increase in error (Walter and Blanch, 2015).

With the error occurring in the clock bias, this fault would typically be concluded as a clock fault, but analysis of the receiver behavior captured by the Wide Area Augmentation System (WAAS) data and independent ground station receivers have suggested that the underlying issue may have affected the code and the carrier components differently. From the reaction of WAAS to the July 10, 2023 event, three overall characteristics were observed initially. There was a code jump accompanied by no carrier phase jump, and an anomaly detected in the signal quality monitor (SQM). The SQM in WAAS first flagged the satellite to be unusable. Given these observations and the continuous tracking maintained throughout the fault, it was speculated that the event was a code-carrier divergence. However, given the fact that L2 was also affected, several IGS receivers were also sampled for its observations of the satellite at the time of fault. At the time of fault, all IGS stations sampled stopped tracking, indicating the likelihood of an anomaly detected in the carrier-phase tracking loop. Such observation indicates an anomaly affecting both the carrier and code phase, suggesting the possible occurrence of a carrier phase cycle slip which went undetected by the WAAS custom G-III receiver. Therefore, the attribution of the fault case as a clock fault due to an error on both code and carrier components without detection of cycle slip on the carrier phase, suggesting an instantaneous jump, is a new case in the history of satellite fault characterizations.

Although we speculate that the signal fault may have had specific properties affecting the code and carrier phase differently, this is difficult to conclude with the initial data evaluated. Because the integer number of wavelengths passed between two points on the carrier phase measurement is typically inferred by the receiver assuming smooth continuous behavior, an abrupt jump in carrier phase may not be accurately captured in receiver data. If the carrier signal itself was discontinuous due to a carrier phase jump, the receiver measurement may become inaccurate, and it may fail to recognize this discontinuity. With the use of carrier smoothing, which is commonly applied to reduce multipath errors and reduce noise in the code phase, discontinuities in the carrier phase with the postulated behavior may be even more difficult to detect. If a cycle-slip also occurs on the carrier phase measurement without a detected loss of phase lock, a satellite clock error could instead be misinterpreted as only a code jump and not recognized as a clock jump . These issues raise the questions of whether all receivers have the capability to capture such high-rate signal transitions, and from an algorithmic consideration, whether such a fault event in these conditions will be attributed to the correct error source. From a safety consideration, knowledge of such differences and therefore the ability to correctly handle these errors in receivers worldwide used for a wide variety of purposes directly affect the safe navigation for civilian and commercial users.

In this paper, we characterize the July 10 and January 25, 2023 fault event through an in-depth analysis of the carrier and code phase data recorded by several receiver stations and the reference receiver of WAAS to draw conclusions on the underlying cause of the fault. Furthermore, high rate data at 100 Hz of the raw correlator outputs are analyzed for the July 10, 2023 fault. This implementation suggests whether the fault occurred due to an isolated code phase jump or if the fault was due to a clock fault and will provide a tool to analyze past and future faults with similar behavior. Finally, we evaluate and provide recommendations based on our findings for whether receiver processing techniques need to be amended in order to provide better accuracy of autonomous satellite performance monitoring within the GNSS constellation.

II. PERFORMANCE EVALUATION PROCEDURE

1. Data Collection

To run the error analysis, several data files from various sources were utilized. The data processing utilized three main datasets: receiver observation data, the precise navigation message, and the broadcast navigation message. The use of these datasets are explained in greater detail in the following subsections. The observation data is collected from the Multi-GNSS Experiment (MGEX) (International GNSS Service, 2012) project spearheaded by the International GNSS Service (IGS) and includes the pseudoranges of the ground station receiver to the satellite. High-rate observation data at one-second sampling rate was used, resulting in 96 files downloaded per day per receiver ground station, as the high rate data is stored in 15-minute increments.

Next, the precise ephemeris and clock products can be downloaded from various institutions, such as the Center for Orbit Determination in Europe (CODE) or the Wuhan University Multi-GNSS experiment (WUM) analysis center. The sinex solution data containing the precise station positions and velocities are provided by the IGS MGEX. Precise corrections for error sources affecting the position solution is also necessary. Specifically, the differential code bias and the precise satellite clock bias values

are provided by the IGS MGEX, and the ionospheric delay corrections can be obtained from the estimates produced by the JPL analysis center.

The broadcast navigation data contains a mulitude of parameters necessary for users to perform positioning and is also provided by the IGS MGEX; specifically, the BRDC broadcast file, which merges the daily broadcast navigation messages from all the receiver stations into a single file, is used for the results obtained in this paper to avoid redundancy between the different broadcast navigation files given by each receiver ground station. However, other methods to obtain this data exists, such as the voting process described by Gunning et al. (2017) which produces a singular broadcast navigation message after internally comparing and culling between all available broadcast messages for the most complete version. In general, many of the historic data files are hosted on a separate website such as the NASA Crustal Dynamics Data Information System (CDDIS). Other analysis centers not mentioned here also provide data files, but those named here are in general amongst the most common. Finally, the antenna phase center offset is necessary and are obtained from the IGS. This results from the fact that the orbit data from the broadcast navigation message are measured to the antenna phase center, but the precise orbit products are measured to the center of mass of the satellite.

2. Precise Point Positioning-Based Fault Monitoring

The real-time error and fault behavior is obtained for potential clock errors using a modified precise point positioning (PPP) model (Lai et al., 2023) with an extended Kalman filter (EKF) that is augmented to include the detection state, denoted as ζ, which represents the clock error. With this modification, the basic equations for this PPP model are:

$$\rho = r + c[\delta t_u - \delta t^s] + I_\rho + T_\rho + \zeta + \varepsilon_\rho \tag{1}$$

where ρ is the pseudorange, r is the geometric range between the receiver and satellite, c is the speed of light, δt_u is the receiver clock bias, δt^s is the satellite clock bias, I_ρ is the ionospheric delay, T_ρ is the tropospheric delay, and ε_ρ contains remaining error corrections, and

$$\phi = \lambda^{-1}[r - I + T] + f \cdot (\delta t_u - \delta t^s) + N + \zeta + \varepsilon_\phi \tag{2}$$

where ϕ is the carrier phase measurement , λ is the carrier wavelength, f is the carrier frequency, I is the ionospheric advance, T is the tropospheric delay, N is the integer ambiguity, and ε_ϕ are the error corrections for the carrier phase measurements (Enge and Misra, 2012). The augmented state matrix, measurement matrix, update equations, and exact handling of error sources are described in detail in Lai et al. (2023) and Lai et al. (2024).

3. Error sources

We use a form of satellite fault monitoring based on PPP described in Lai et al. (2023). To obtain the real-time GPS fault event, several corrections need to be included in the model. In general, error sources caused by satellite performance include, but are not limited to, satellite clock and ephemeris errors, ranging signal deformation errors, biases between signals at difference frequencies, and incoherence between the signal code and carrier. Other error sources not directly due to the performance of the satellite include ionospheric and tropospheric errors, noise and interference, receiver antenna biases, receiver antenna group delay, and multipath.

In particular, receiver antenna phase center offset and variation, tropospheric and ionospheric delay, carrier phase windup, satellite clock relativistic time offset, solid Earth tides, ephemeris errors, and satellite clock and differential code biases are included in the PPP model used here.

III. GPS SERVICE HISTORY

Several past papers have characterized the performance of the GPS constellation. In particular, Walter and Blanch (2015) showed that during a seven-year period from the start of 2008 to the end of 2014, five faults were identified, each on different satellites, with a roughly even distribution of clock and orbital faults. Although the earliest fault identified on SVN 25 on June 26, 2009 was the only case to exhibit an instantaneous clock error, the analysis from the 2015 paper was only extended to a 15 minute sampling rate, and it is unclear whether the clock error would still exhibit this instantaneous onset behavior at higher sampling rates. Wang and Walter (2023) continued to characterize faults on the GPS constellation, demonstrating that between 2012 and early 2022 at the time of publication, there were no new GPS faults, but that from 2017 until 2021, several "near-fault" events presented. In late 2022, on October 2, 2022, a sixth fault occurred since the Walter and Blanch (2015) fault evaluation, ten years later. This fault occurred on SVN 58 (PRN 12) and was a small clock ramp lasting 45 minutes and reaching a maximum error only a few meters larger than the fault definition. SVN 58 self-corrected after a new issue of data: clock (IODC) upload

before it could be set as unhealthy (Wang and Walter, 2023). This can be expected, as satellites can worsen as they age from their launch date.

However, what is unexpected are the three anomalous events that occurred on the same GPS satellite, SVN 63, in 2023, with two being official faults. Specifically, Lai et al. (2023) showed two faults occurring on January 25 and July 10 and an anomaly occurring on January 28. Interestingly, these errors all presented as instantaneous clock faults using a one-second sampling rate, a rare case in the history of previous GPS fault causes. The following section will go into detail on the onset of the July 10, 2023 fault and observed behavior to inform future design updates.

IV. SVN 63 JULY 10, 2023 FAULT

The following subsections describe the observations of the July 10, 2023 fault occurring on SVN 63. First, data from the WAAS G-III receiver is shown, where signal tracking was maintained throughout the event. Data from a handful of IGS stations from different receiver manufacturers are also shown as well as the locations of these stations with respect to the satellite location. Furthermore, raw correlator measurements and both IQ correlator data and carrier-differenced data at 100 Hz are provided to further describe the signal quality near the time of fault.

1. July 10, 2023 WAAS G-III Receiver Performance

On July 10, 2023, the NovAtel G-III receivers used by the WAAS observed a rapid code phase of -40 m within roughly 6 seconds. The observed clock ramp began on 09:57:17 GPS Time (GPST) and exceeded the fault definition only two seconds later at 09:57:19 GPST, or 09:56:59 UTC. By 09:57:24 GPST, the clock error observed by the WAAS G-III receivers settled at approximately -40 m. Five seconds later, WAAS flagged the satellite as unusable at 09:57:22 GPST. According to the Notice Advisory to Navstar Users (NANU), a message which is issued by the GPS Operations Center and the United States Coast Guard providing status updates on the health of individual GPS satellites, SVN 63 was set to the unhealthy state at 10:02:00 GPST, nearly five minutes after the fault occurred. The satellite was never set back to healthy and was decommissioned approximately one month later, on August 10, 2023.

The G-III receivers have a code-loop tracking bandwidth of 0.2 Hz and took about five seconds to settle to the final -40 m change. The carrier loops exhibited continuous tracking without a corresponding 40 m change. We suspected that the true satellite fault was an instantaneous 40 m clock jump and that the carrier loop failed to track and which affected the code loop's ability to follow immediately. To test this theory, Zeta Associates simulated a -40 m clock fault on both the code and carrier and injected this into a G-III receiver at their facility. Figure 1 shows the code minus carrier data capturing the fault behavior by the G-III receiver at the ZDC station site. As can be seen, the G-III receiver maintains lock on the signal throughout the event. Although a one second sampling rate is considered high-rate, the simulation allowed the step to be injected precisely at time of week (TOW) of 122236, or 09:57:16 GPST, and was necessary to further suggest the fault cause as an instantaneous error at this specific time. The red plot in Figure 1 is the simulated result, exhibiting a near identical match to the real event observed. Therefore, we believe that SVN 63's clock did actually change to -40 m within one second, and the carrier tracking loops failed to recognize this change which in turn prevented the code-tracking loops from immediately following this clock jump. At the time of fault, the broadcast user range accuracy (URA) was 3.4 m giving a fault definition of 15.03 m. Therefore, Figure 1 reflects a fault occurring at 09:57:19 GPST, at the first data point exceeding -15 m, but it should be noted that the fault definition in reality was exceeded at the time of the instantaneous clock step, at 09:57:16 GPST.

Receiver Type	Station Name	Signal Loss Start Time	Signal Loss End Time	Duration of Signal Loss (s)
Septentrio PolaRx5	HLFX	09:57:16	09:57:26	11
Septentrio PolaRx5	QAQ1	09:57:16	09:57:26	11
Septentrio PolaRx5	SCOR	09:57:16	09:57:26	11
Trimble Alloy	UNB3	09:57:16	09:57:19	4
Trimble Alloy	FUNC	09:57:16	09:57:19	4
Trimble Alloy	CPVG	09:57:16	09:57:19	4
JAVAD TRE_3 Delta	GODN	09:57:16	09:57:19	4
JAVAD TRE_3 Delta	PIE1	09:57:16	09:57:19	4
JAVAD TRE_3 Delta	BOGT	09:57:16	09:57:20	5

Table 1: Receiver tracking behavior from different ground stations for July 10, 2023

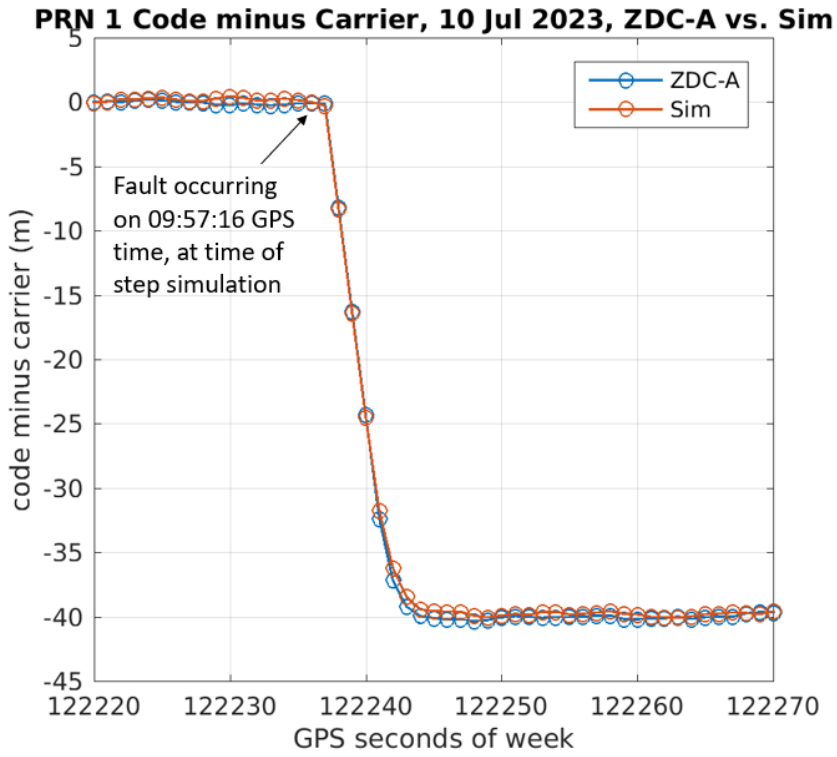

Figure 1: Real and simulated fault behavior on SVN 63 from the G-III receiver, provided by Zeta Associates.

2. July 10, 2023 Fault Comparison to IGS Receivers

In order to distinguish between the true satellite signal behavior and the corresponding receiver responses, the July 10, 2023 fault behavior was obtained by applying the PPP method described earlier across multiple receiver stations encompassing three different receiver models in order to obtain the signal behavior in real time during the time of the event. Specifically, the three receiver models used were the Septentrio PolaRx5, the Trimble Alloy, and the JAVAD TRE_3 Delta. Table 1 shows the stations chosen for each receiver model type as well as the signal loss and start times in GPS Time and the duration of signal loss in seconds.

Figure 2 shows on average a better geometry of the satellite to the Trimble Alloy and JAVAD TRE_3 Delta receiver stations sampled at the time of error. Figures 3-5 are the real-time fault behavior obtained from each of these receivers sampled. The red crosses plotted represent missing data for that time step. Figure 3 shows the fault behaviors obtained by the Septentrio PolaRx5 receiver types. Although two of the three receivers sampled reach a maximum error of -40 m, results from the HLFX station show an initial error greater than -60 m at the beginning of the fault. Furthermore, the receiver stations sampled for this receiver

type shows an identical 11 seconds of signal loss.

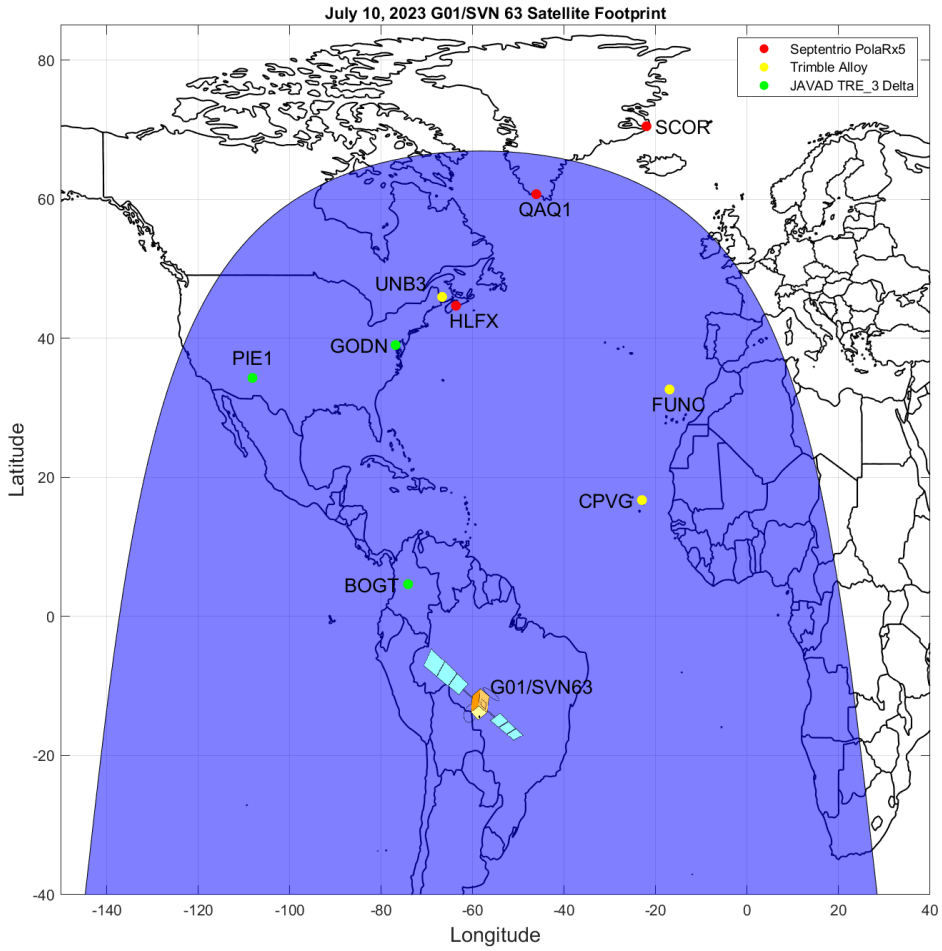

Figure 2: Map of IGS reference ground receivers sampled and satellite footprint of SVN 63 (GPS 1) on July 10, 2023 near time of instantaneous clock jump.

Figures 4 and 5 appear to exhibit very similar behavior in reaction to the sudden clock jump event. The duration of signal loss are all 4 seconds with the exception of the BOGT ground station receiver. The settling error of the fault are also all around -40 m for these ground receivers.

It can be seen through Figures 3 and 5 and more straightforward in Table 1 that receivers of the same manufacturer and model tend to perform similarly to each other. Furthermore, despite the differences observed, the onset behavior in the few seconds leading up to the fault show identical behavior across all ground station receiver types sampled. Not a single IGS ground station was able to track through the code jump, unlike the G-III receiver performance which maintained signal tracking throughout.

In comparison to Figure 1 provided by Zeta Associates, the onset and settling error of the fault are similar in behavior. It can also be seen that the ground station receivers lose signal right when the instantaneous clock jump occurred, at 09:57:16 GPST, as described earlier in the simulation using the G-III receiver data shown in Figure 1. Because all IGS stations lost code and carrier lock between 09:57:15 GPST and 09:57:19 GPST, none were able to characterize the clock behavior over that time interval. However, all observations are consistent with the presumed sudden transition between 09:57:17 GPST and 09:57:18 GPST.

3. July 10, 2023 Prompt Correlator Data at 1 Hz

Figure 6 shows 1 Hz data of the raw correlator measurements during the few seconds before and after the apparent fault time. Note that the nine correlator taps from SQM 0 to SQM 8 are taken at the same time for each second that has passed by, but are plotted with 0.025 s offsets, with the 0 chip prompt centered at the top of the second to more clearly demonstrate the correlation peaks expected. In general, when the signal is well-matched, we expect the correlation to be lower at the “earliest” (SQM 0)

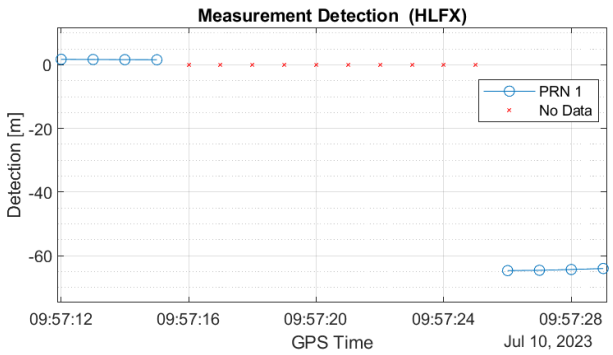

(a) HLFX Station

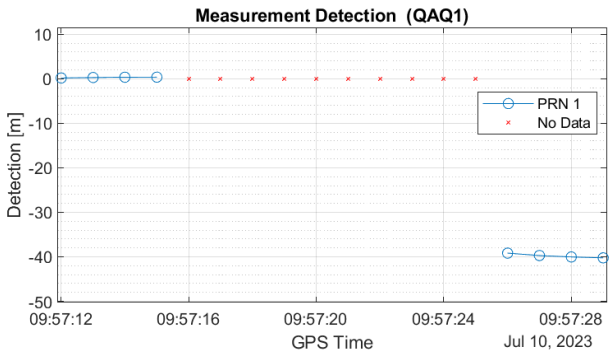

(b) QAQ1 Station

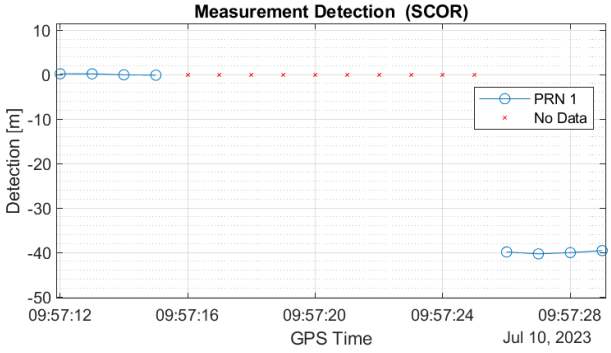

(c) SCOR Station

Figure 3: Real-time fault onset behavior of Septentrio PolaRx5 receiver types on July 10, 2023.

and "latest" (SQM 8) chips and the highest correlation to be found at the time-aligned prompt replica (SQM 4). This behavior is seen at times 09:57:14-16 and 09:57:22-24 GPST, although at 09:57:16 GPST there is a drop in the correlator accumulations. During 09:57:17 - 09:57:19 GPST, the received signal and the replica signal in the ground receiver are completely mismatched as can be seen by the earliest correlator taking the highest accumulations. This is consistent with a shift of the correlation peak to the left as would be caused by a -40 m clock jump. At 09:57:20-21 GPST, the receiver is already beginning to attempt locking back onto the signal.

4. July 10, 2023 High Rate IQ Correlator and Carrier Phase Data at 100 Hz

In Figure 1, it can be seen that simulating a -40 m clock jump on both the code and carrier range at 09:57:16 GPST resulted in a near identical match of the satellite performance captured by the G-III receiver. Figure 6 at 09:57:16 GPST shows a well-matched signal, aside from the accumulation drop. Figure 7 shows the decomposed I and Q correlator data for L1 at an even finer sampling rate of 100 Hz. At 09:57:15.48 GPST, there is a drop in observed power, and at 09:57:15.79 GPST, the receiver stops reporting altogether. At 09:57:16.30 GPST, the receiver begins reporting again and attempts to lock onto the received signal. Around 09:57:17.05 GPST, the signal is locked on for roughly a half of a second, until 09:57:17.60 GPST, one-tenth of a second after what is shown in Figure 7, when the receiver stops reporting altogether again. After a little over 8 s, the receiver begins reporting information with seemingly normal signal lock again at 09:57:25.90. The bottom graph in Figure 7 shows the time difference of the carrier phase, which is the difference between the current time step carrier phase measurement and the preceding carrier phase measurement. We expect there to be a small increasing or decreasing change in this value as the satellite passes over the ground receiver in its orbit, such as in the behavior shown in the bottom plot of Figure 7 at 09:57:15.00 - 09:57:15.47 GPST. After 09:57:15.48 GPST, it can be seen that the carrier phase measurement obtained is abnormal.

Figure 8 shows the same I and Q correlator data but for L2 from the same time period at 100 Hz. Here, the I and Q correlator on the L2 band loses power at 09:57:15.47 GPST, attempts to lock onto the signal right after 09:57:16.08 GPST before stopping reporting altogether at 09:57:16.88 GPST. The receiver begins reporting data again on the L2 band at 09:57:24.88 GPST, as seen in Figure 10.

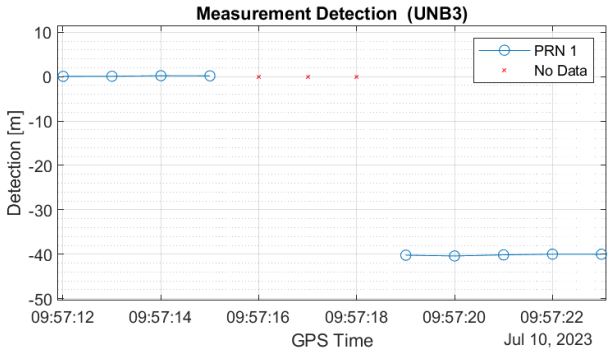

(a) UNB3 Station

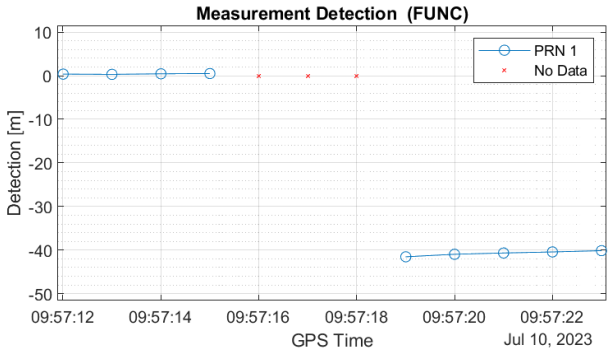

(b) FUNC Station

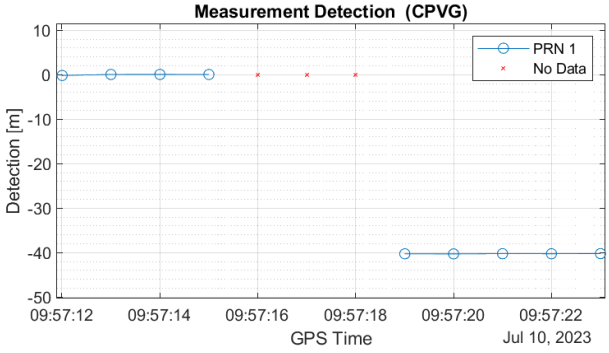

(c) CPVG Station

Figure 4: Real-time fault onset behavior of Trimble Alloy receiver types on July 10, 2023.

V. SVN 63 JAN 25, 2023 FAULT

The following subsections describe the observations of the January 25, 2023 fault occurring on SVN 63. Again, data from the WAAS G-III receiver is shown first, where signal tracking was maintained throughout the event. Finally, data from a handful of IGS stations from different receiver manufacturers are also shown as well as the locations of these stations with respect to the satellite location.

1. Jan 25, 2023 WAAS G-III Receiver Performance

The performance of the fault which occurred on January 25, 2023 on SVN 63 captured by the WAAS NovAtel G-III receiver at the Honolulu, Hawaii station is shown in Figure 11. The blue plot shows the code minus carrier range measurements for the L1 band and the red plot shows the same for the L2 band. At 16:02:45 GPST, the code phase begins a rapid descending ramp before approaching the settling error. Taking an average of this data, we see that the settling error after the fault occurs is approximately -27 m. The lower bandwidth of the L2 signal as compared to the L1 signal may be a contributing factor for the apparent lag in reaction of the L2 data. More importantly, we see that the anomalous event has affected both the L1 and L2 signals similarly.

2. January 25, 2023 Fault Comparison to IGS Receivers

To investigate the satellite fault cause and eavluate the response by WAAS, similar to the July 10, 2023 analysis, we identify a handful of IGS stations to compare receiver performance with. Figure 12 shows the locations of these IGS ground receivers in relation to the location and footprint of SVN 63 on January 25, 2023. Due to the location of the satellite being mainly over a body of water, the IGS receivers sampled here are four Septentrio PolaRx5 receivers, three Trimble Alloy receivers, and two Trimble NETR9 receivers. All the satellites stop reporting at 16:02:41 GPST. In Figure 13, we see that for the Septentrio PolaRx5 receivers, three of the four receivers sampled experience 9 s of lack of reporting. However, two of the receivers report a settling error of approximately -53 m, with the other two receivers reporting approximately -20 and -27 m settling error after the fault.

Figure 14 shows the satellite signal behavior near the time of fault on January 25, 2023 captured by the Trimble Alloy receivers.

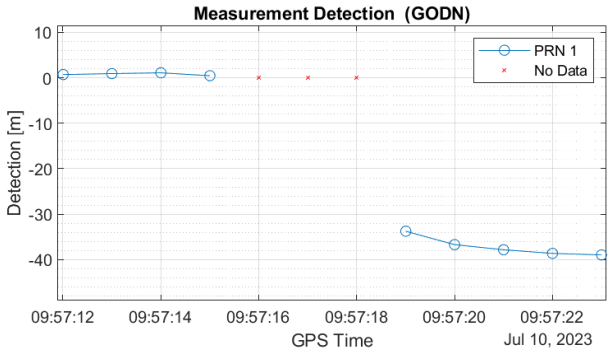

(a) GODN Station

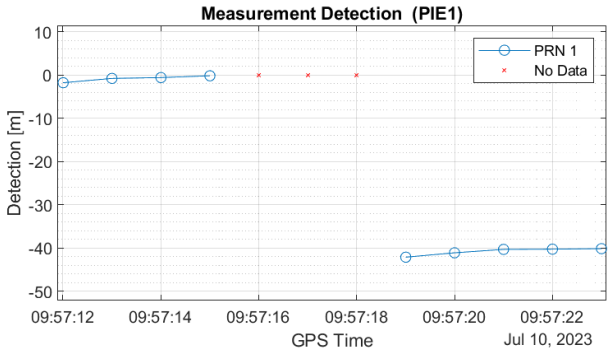

(b) PIE1 Station

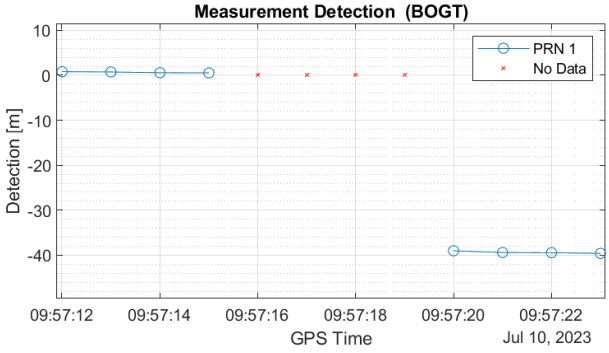

(c) BOGT Station

Figure 5: Real-time fault onset behavior of JAVAD TRE_3 Delta receiver types on July 10, 2023.

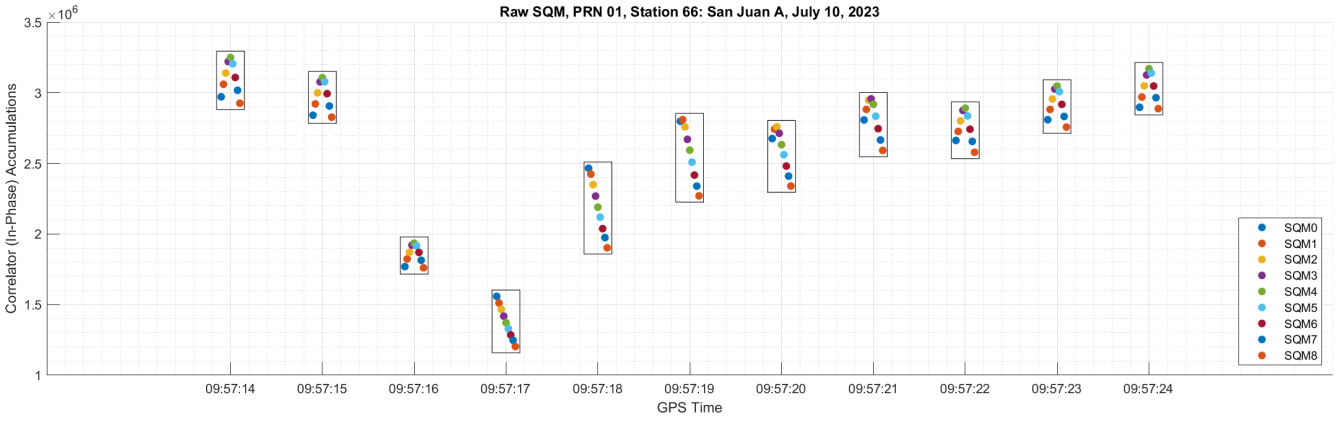

Figure 6: Raw correlator data showing the signal mismatch at time of fault.

A seven second signal reporting loss occurred and the clock error observed were all just under -30 m, similar to the observations of Figure 11.

For the last receiver model sampled, the Trimble NETR9 receiver types showed a wide range of recovery times after signal loss started at 16:02:41 GPST. The IGS station in Tahiti (THTI) begins reporting again after 5 s, while the IGS station in the Cook Islands (CKIS) begins reporting after 12 s. Both stations reported just under -30 m of clock error, which is similar to the data tracked by the WAAS receiver sampled.

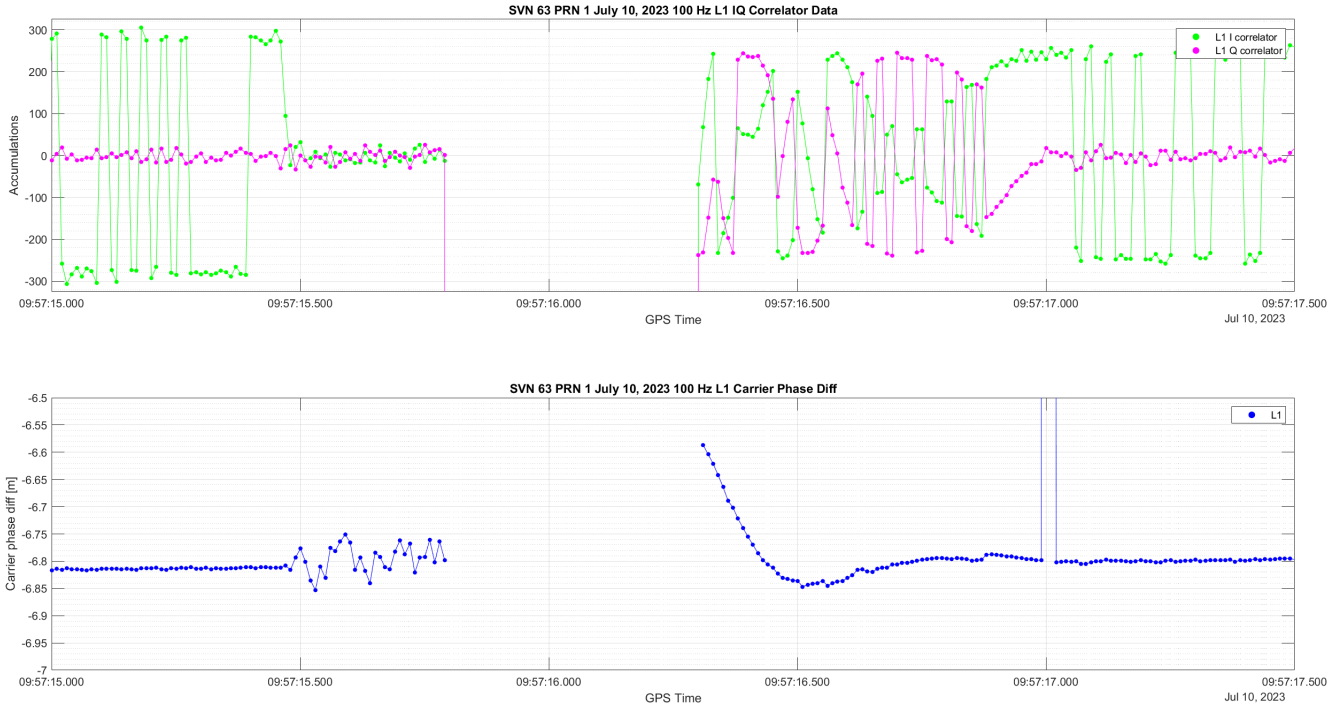

Figure 7: IQ correlator and carrier-differenced data on L1 at 100 Hz during July 10, 2023 fault onset.

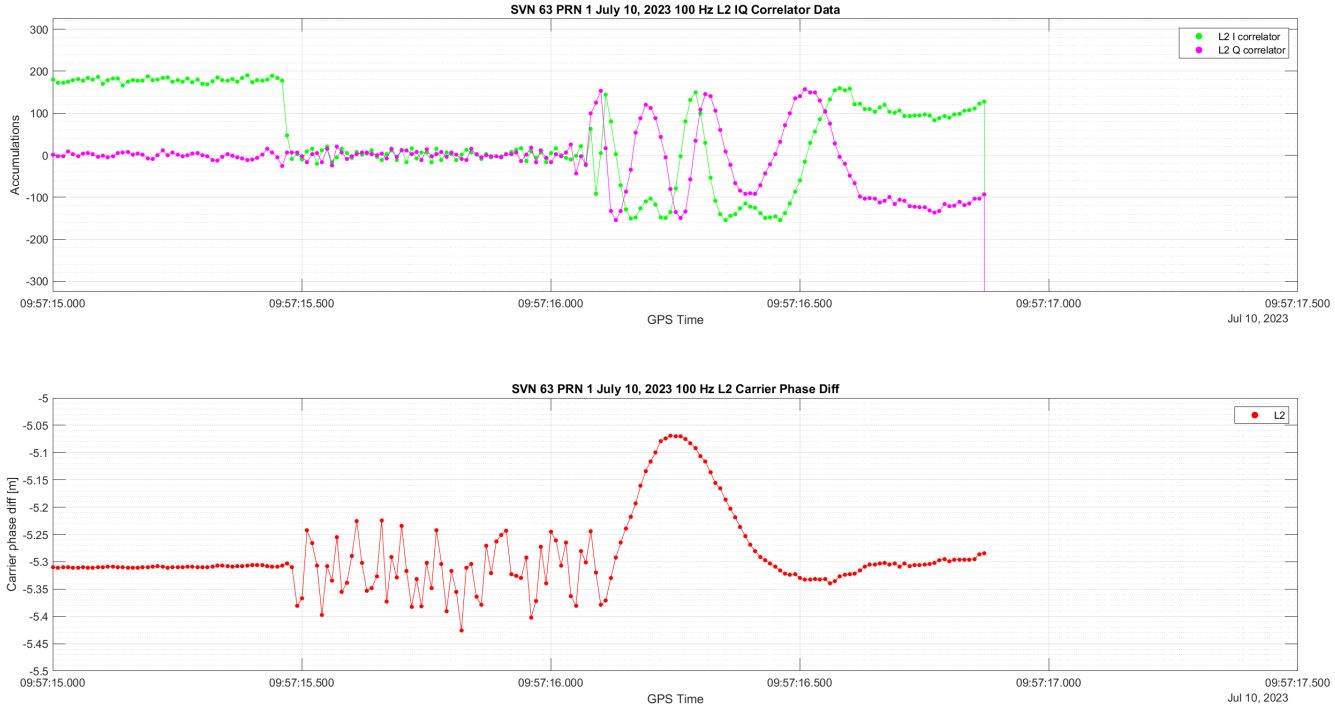

Figure 8: IQ correlator and carrier-differenced data on L2 at 100 Hz during July 10, 2023 fault onset.

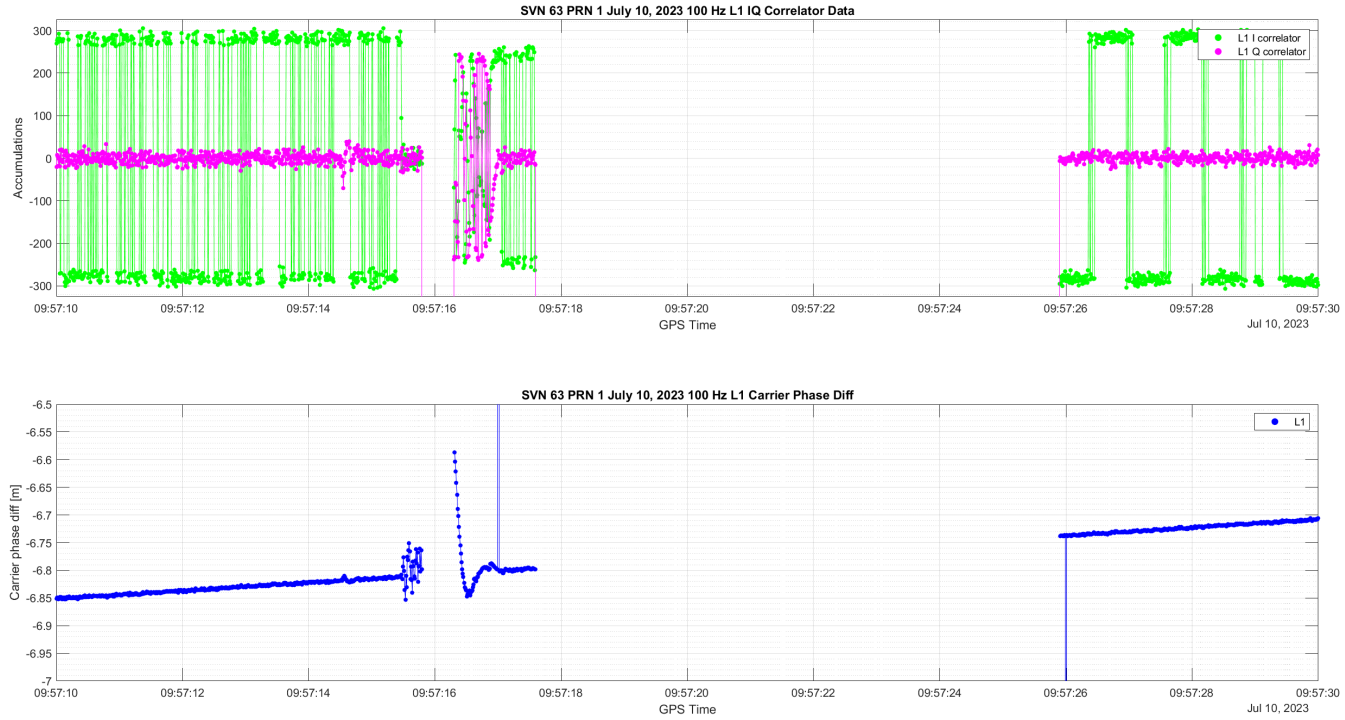

Figure 9: Zoomed out IQ correlator and carrier-differenced data on L1 at 100 Hz during July 10, 2023 fault onset.

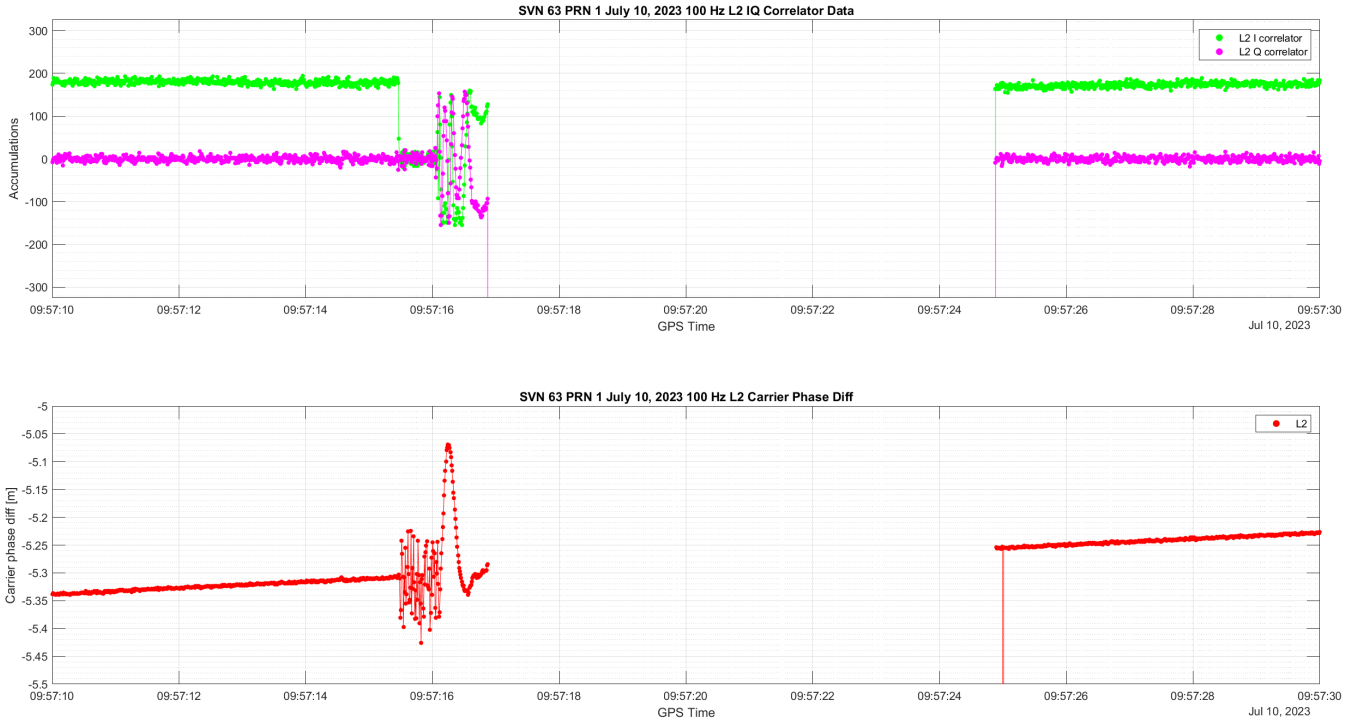

Figure 10: Zoomed out IQ correlator and carrier-differenced data on L2 at 100 Hz during July 10, 2023 fault onset.

VI. FAULT CAUSE AND RECEIVER PROCESSING DIFFERENCES

The apparent loss of lock in the IGS ground station receivers but continued signal lock by the G-III receiver during the instantaneous 40 m and 27 m code and carrier step indicates a difference in the signal tracking methods of the different receivers'

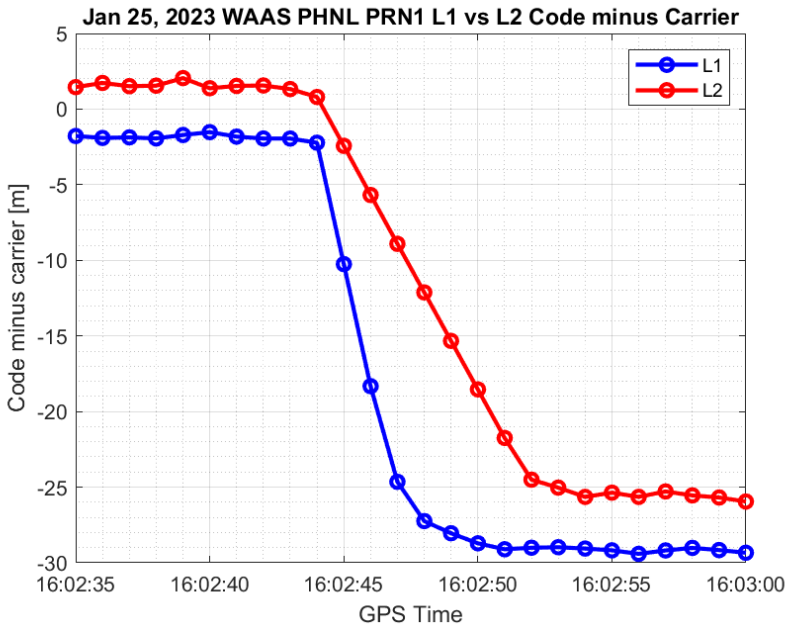

Figure 11: January 25, 2023 WAAS NovAtel G-III Receiver L1 and L2 data.

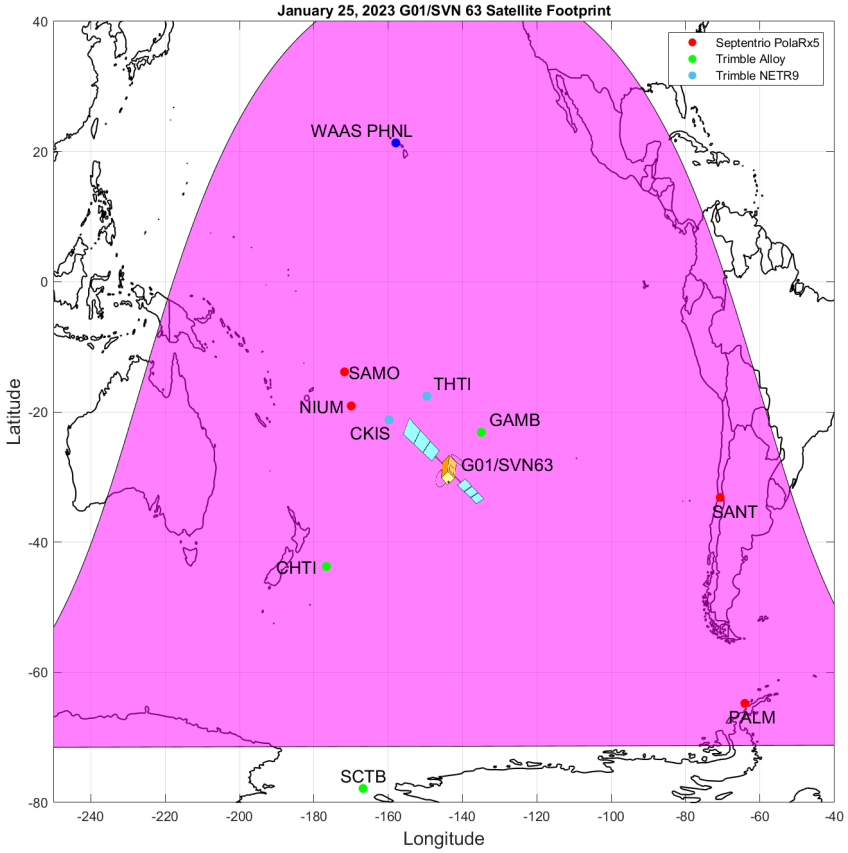

Figure 12: Map of IGS reference ground stations sampled, WAAS station, and satellite footprint of SVN 63 (GPS 1) on January 25, 2023 near time of fault.

Receiver Type	Station Name	Signal Loss Start Time	Signal Loss End Time	Duration of Signal Loss (s)
Septentrio PolaRx5	SANT	16:02:42	16:02:45	4
Septentrio PolaRx5	PALM	16:02:42	16:02:49	8
Septentrio PolaRx5	NIUM	16:02:42	16:02:49	8
Septentrio PolaRx5	SAMO	16:02:42	16:02:49	8
Trimble Alloy	GAMB	16:02:42	16:02:47	6
Trimble Alloy	SCTB	16:02:42	16:02:47	6
Trimble Alloy	CHTI	16:02:42	16:02:47	6
Trimble NETR9	THTI	16:02:42	16:02:45	5
Trimble NETR9	CKIS	16:02:42	16:02:52	11

Table 2: Receiver tracking behavior from different ground stations for January 25, 2023

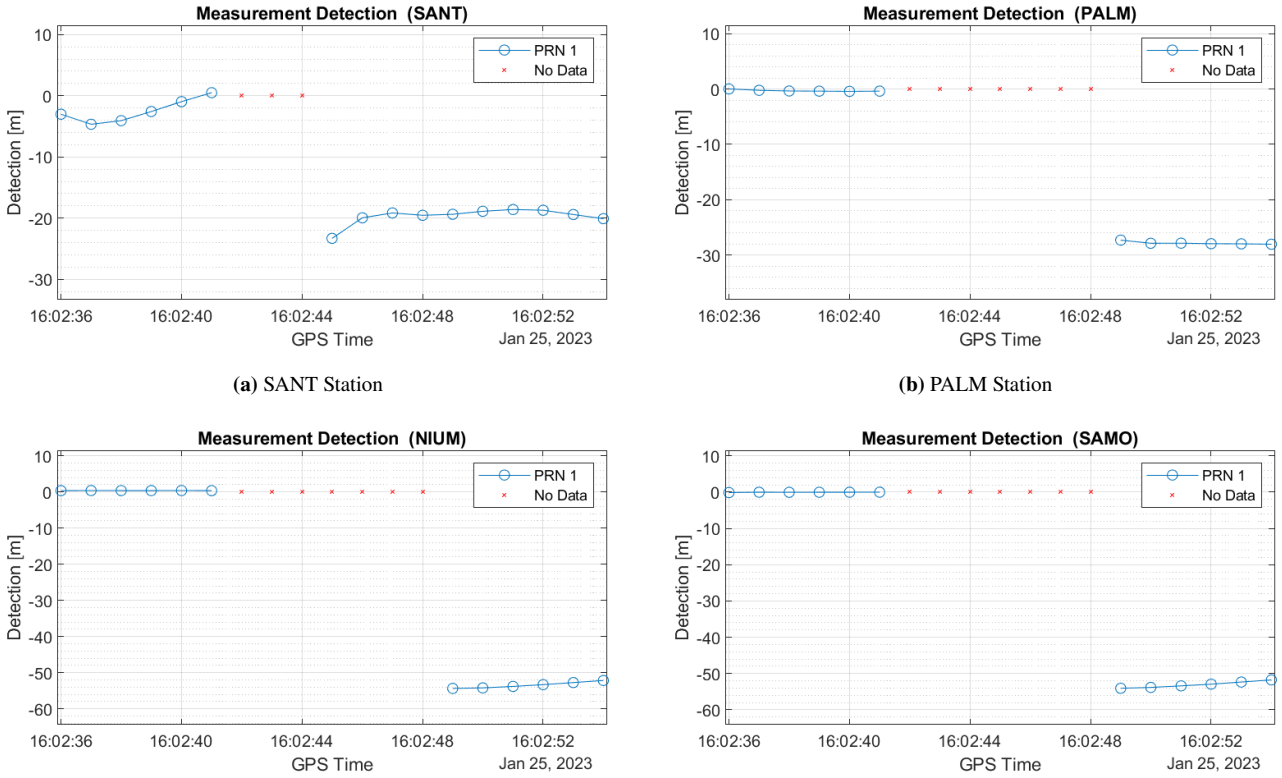

(a) SANT Station

(b) PALM Station

(c) NIUM Station

(d) SAMO Station

Figure 13: Real-time fault onset behavior of Septentrio PolaRx5 receiver types on January 25, 2023.

carrier tracking loops. Carrier smoothing, which is used to mitigate the noisiness of measurements, can lead to anomalous error events due to the apparent code-carrier divergence. The G-III carrier phase measurements are particularly concerning as they did not reflect the large clock jumps. As a consequence these clock jumps were also not present in the resulting carrier smoothed output. Fortunately all of the other receiver types exhibited a loss of lock associated with the clock jump and therefore their carrier smoothing would have reset and thus properly reflect the large clock jumps.

As mentioned much earlier in the introduction section of this paper, the high frequency and large quantity of carrier phase wavelengths passing through per each time step of the receiver sampling rate indicates that, in rare cases, extreme anomalous events may not be detected in the carrier phase measurement if the event occurs such that the last measured carrier wave cycle position correlates with the expected carrier wave cycle position to be seen at the next time step, despite the now incorrect number of integer cycles recorded by the receiver. The WAAS reference receivers maintain phase lock despite an abrupt change on the carrier wave, but was still able to flag users to stop using the PRN 1 signal from SVN 63 based on anomalous measurements

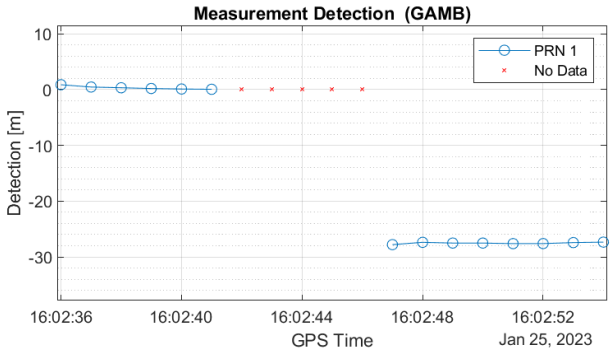

(a) GAMB Station

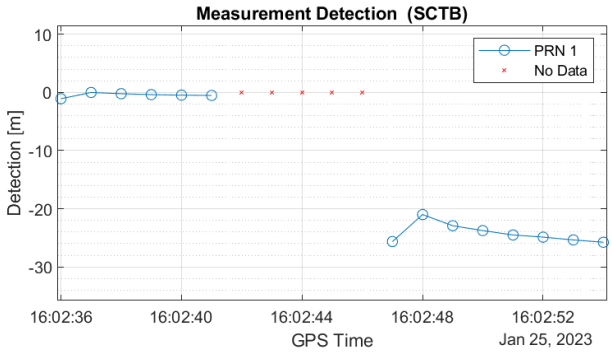

(b) SCTB Station

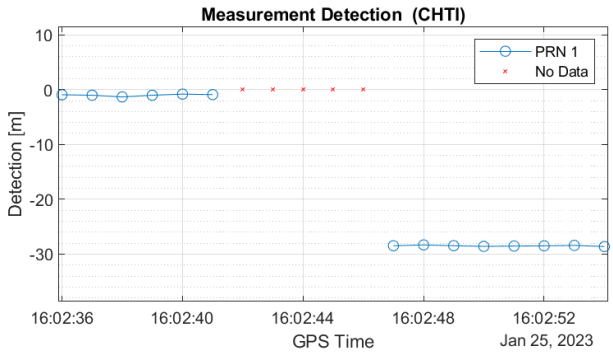

(c) CHTI Station

Figure 14: Real-time fault onset behavior of Trimble Alloy receiver types on January 25, 2023.

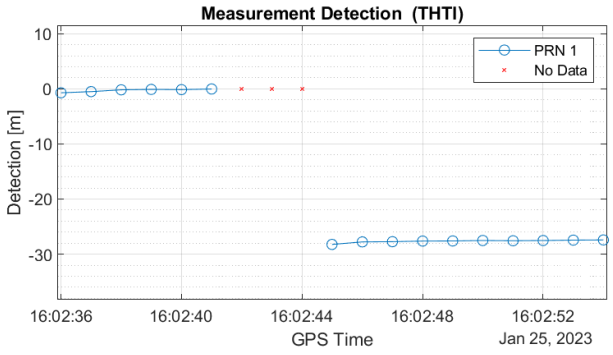

(a) THTI Station

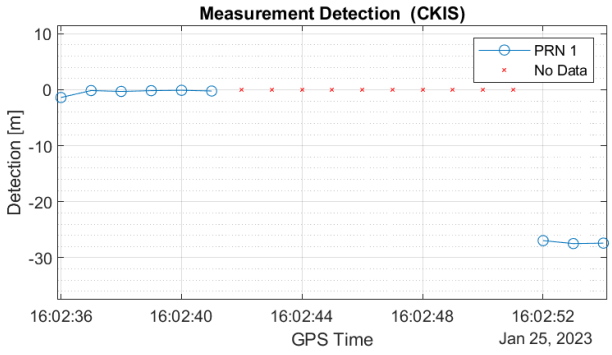

(b) CKIS Station

Figure 15: Real-time fault onset behavior of Trimble NETR9 receiver types on January 25, 2023.

detected at 09:57:17 GPST. Note, the decision to alert was made using data from 09:57:17 GPST, but the user was not alerted until five seconds later at 09:57:22 GPST. This is not due to the code or carrier measurements made, but rather in the signal quality monitor (SQM), which detected significant signal deformation when the clock jump occurred. Important to note is that the G-III receiver provided by NovAtel for WAAS has many non-standard design specification per requests of WAAS designers. This offers insight as to why the G-III receiver behaved differently throughout the event as compared to other reference receivers and a potential reasoning for why the G-III receiver was able to continue providing measurements throughout. The January 25, 2023 fault also exhibited similar behavior, with the WAAS G-III receiver tracking throughout the fault. Although there is wide variability in signal trackingk in the various IGS receivers, they all stop tracking at 16:02:41 GPST.

VII. CONCLUSION

This research suggests an instantaneous clock jump caused the July 10, 2023 fault on SVN 63. Furthermore, this new fault case has led to further analysis suggesting that not all receivers react similarly to anomalous satellite events. Specifically, different error sources may elicit a variety of reactions from different receivers. This clock fault which occurred as an instantaneous clock jump in both the code and carrier, but which was undetected in the carrier tracking loop of the G-III receiver, resulted in a variety of signal tracking performance issues when the jump occurred. The NovAtel G-III custom receiver used in WAAS is able to detect an anomaly from an erroneous behavior detected by its SQM feature at 09:57:17 GPST, notifying users at 09:57:22 GPST. For the IGS ground station reference receivers, it is likely that internal tracking loop logic caused the other examined makes of receiver to discontinue tracking of the PRN 1 signal from SVN 63 until seconds later. This event draws attention to the importance of robust signal tracking logic since varying logic will affect the receiver's response and affect whether a user uses a healthy or compromised satellite. Applying similar steps, processing data for the January 25, 2023 fault revealed similar behavior in which the WAAS G-III custom-designed receiver maintained tracking throughout the clock event, providing code phase measurements throughout the fault, while IGS receiver stations in view of the satellite experience a few-second signal loss duration before reporting again. In the future, it would be informative to obtain higher sampling rate data for the January 25, 2023 fault, and to simulate steps and ramps at the onset of the January 25, 2023 fault and the January 28, 2023 anomaly to investigate which component of the event, mainly the code, carrier, or signal deformation feature, triggered the receiver's response to the event. This would provide a more complete picture and insights to other edge cases which can inform more robust signal tracking design.

ACKNOWLEDGEMENTS

We gratefully acknowledge the support of the FAA Satellite Navigation Team for funding this work under Memorandum of Agreement #: 693KA8-22-N-00015.

REFERENCES

Department of Defense (2020). Global Positioning System Standard Position Service Performance Standard, 5th Edition, April 2020.

Enge, P. and Misra, P. (2012). Global Positioning System: Signals, Measurements and Performance, Revised Second Edition (Paperback).

Gunning, K., Walter, T., and Enge, P. (2017). Multi-GNSS Constellation Anomaly Detection and Performance Monitoring. In *Proceedings of the 30th International Technical Meeting of the Satellite Division of The Institute of Navigation (ION GNSS+ 2017)*, pages 1051–1062. ISSN: 2331-5954.

International GNSS Service (2012). Multi-GNSS Experiment.

Lai, Y.-F., Blanch, J., and Walter, T. (2024). Range Error Bounds with Integrity for PPP. In *2024 International Technical Meeting of The Institute of Navigation*, Long Beach, California.

Lai, Y.-F., Blanch, J., Walter, T., Kahr, E., Leahy, E., Silva, P., and Ellum, C. (2023). Prototyping Integrity Monitors for PPP Fault Detections. In *36th International Technical Meeting of the Satellite Division of The Institute of Navigation (ION GNSS+ 2023)*, pages 2592–2605, Denver, Colorado.

Walter, T. and Blanch, J. (2015). KEYNOTE - Characterization of GNSS Clock and Ephemeris Errors to Support ARAIM. In *Proceedings of the ION 2015 Pacific PNT Meeting*, pages 920–931. ISSN: 2331-6284.

Wang, R. and Walter, T. (2023). Characterization and Comparison of Galileo and GPS Anomalies. In *2023 International Technical Meeting of The Institute of Navigation*, pages 597–610, Long Beach, California.